

# Quasicrystalline d-AlCuCo identified as random tiling by ion channeling combined with particle induced X-ray emission

Gabriele Zeger, Dieter Plachke<sup>†</sup>, Heinz Dieter Carstanjen<sup>†</sup>, and Hans-Rainer Trebin  
*Institut für Theoretische und Angewandte Physik, Universität Stuttgart  
Pfaffenwaldring 57, D-70550 Stuttgart, Germany*

<sup>†</sup> *Max-Planck-Institut für Metallforschung, Heisenbergstr.1, D-70569 Stuttgart, Germany*

In a model quasicrystal for decagonal AlCuCo the phason disorder was gradually increased and the channeling PIXE yields were computed for 3 MeV He ions by Monte Carlo simulations. For large phason disorder good agreement with experimental data was obtained. Thus we conclude that the sample of d-AlCuCo used in the measurements is a random tiling. One remaining discrepancy, namely that the PIXE yields of the simulations are approximately the same for Cu and Co, is eliminated by optimization of the Cu and Co positions.

One of the fascinating challenges in quasicrystal research is to distinguish where quasiperiodicity reproduces properties of periodic crystals and where it leads to new phenomena. An interesting *new* aspect is the phason degree of freedom. When a quasicrystal is described by the atomic decoration of a quasiperiodic tiling such as the well known Penrose Tiling [1] or its decagonal partner, the Tübingen triangle tiling [2], phason motion becomes evident in the form of simpleton flips of vertices, in the Penrose pattern within a hexagon, in the triangle tiling within a rhombohedron. Katz and Kalugin suggested that phason flips induce a new mode of selfdiffusion [3–5]. Recent measurements of the diffusion constant in i-AIPdMn indeed indicate that low-temperature diffusion occurs via a phason assisted mechanism [6]. Phasons also can transform a quasiperiodic tiling into a rational approximant [7] or a random tiling [8].

In the following we will concentrate on another aspect of phason disorder, namely how it influences channeling PIXE-profiles in the specific case of decagonal AlCuCo. This has been the first T-phase to be grown from the melt up to mm-sized thermodynamically stable single crystals. Detailed structure analyses have been performed of d-AlCuCo and the isostructural phase d-AlNiCo [9–11]. Evaluating the intensity of 30,000 Bragg Peaks of AlCuCo and performing a Patterson analysis Steurer obtained an electron density distribution and the positions of 20,000 atoms in a patch [12]. From these measurements several model quasicrystals were derived according to which AlCuCo and AlNiCo consist of two plane decagonal quasicrystalline layers, alternatively stacked along a perpendicular tenfold screw axis with a stacking period of 4.18 Å [14]. On the basis of Steurer’s data Burkov proposed a tiling model for AlCuCo, first resting on a cluster decoration of the Penrose tiling [15], in a second variation on a decoration of the Tübingen triangle tiling [16].

The first-hand information of Steurer’s experiments is on the structure in reciprocal space. Thus it appears natural

to test the models derived from the data by an experiment in direct space. Carstanjen *et al.* performed fast ion channeling on d-AlCuCoSi combined with Rutherford backscattering (RBS) to study the decoration of the T-phase structure in real space [17,18]. Cu and Co on one side and Al and Si on the other could not be distinguished because their mass differences are too small [19,21]. Monte Carlo computer simulations of RBS-yields on both Burkov models and on one set of data from Steurer differed significantly from the experiments [21]. In Burkov’s models Cu and Co atoms are distinguished via matching rules of the Tübingen triangle tiling. To test this distribution of chemical species the characteristic ion induced  $K_{\alpha}$ -X-ray emission (PIXE) was measured [21]. The yield profiles (Fig. 4) show a significant difference for Cu and Co which, as we will see, cannot be confirmed by Burkov’s models.

Since X-ray investigations of both T-phases by Frey and Steurer [22] display an appreciable diffuse background and thus are indicating a large amount of disorder, it is necessary to study not only deterministic models of AlCuCo, but also models with phason disorder. Recently we have presented a model of d-AlCuCo, in which it is possible to introduce phason disorder in the form of flips [23].

Using this model we will show how a certain amount of phason disorder changes the PIXE-yields and leads to good agreement with the experimental data. The only discrepancy is that the PIXE-yields turn out to be approximately the same for Co and Cu. We eliminate this deficiency by modifying the Co- and Cu-positions and the chemical composition [24]. Since both the influence of phasons and the distribution of Co and Cu can be discussed for PIXE-yields, the RBS simulations will be presented in a future paper [27].

The two Burkov models (BI and BII) and our modifications thereof (MI and MII) are atomic decorations of the Tübingen triangle tiling. There are four atomic surfaces, two for each layer. For all models those of the first layer

belong to the translational classes  $T=1$  and  $3$  and are depicted in Fig. 1 [28]. The atomic surfaces for the second layer belong to  $T=2,4$  and are copies thereof rotated by an angle of  $2\pi/10$  due to the generalized tenfold screw axis of the quasicrystal. For BII and MII the atomic surfaces of translational class  $T=1,4$  are purely occupied by Al and form a symmetric pentagonal star. The atomic surfaces of  $T=2,3$  are decagons. With the polar calculus [29] the composition is calculated to  $\text{Al}_{62}\text{Cu}_{19}\text{Co}_{19}$  for BI and BII and to  $\text{Al}_{62}\text{Cu}_{24}\text{Co}_{14}$  for MI and MII. BI and BII predict the “magic composition”  $\text{Al}_{\tau-1}\text{Cu}_{\tau-2/2}\text{Co}_{\tau-2/2}$  where  $\tau$  denotes the golden mean  $(1 + \sqrt{5})/2$ . Since for the RBS- and PIXE-experiments a sample of composition  $\text{Al}_{62}\text{Cu}_{20}\text{Co}_{15}\text{Si}_3$  has been used we not only changed the positions of several Cu- and Co-atoms but also their concentrations in constructing models MI and MII. With a composition of  $\text{Al}_{\tau-1}\text{Cu}_{\tau-3}\text{Co}_{\tau-4}$  they are in a certain way also “magic”.

In MI and MII the core of the  $T=3$  atomic surface is occupied by Co atoms. The shortest Co-Co distance is  $4.46 \text{ \AA}$  whereas small Cu-Cu distances with  $2.58 \text{ \AA}$  and  $2.89 \text{ \AA}$  are frequent. It is a remarkable feature of MI and MII that the pure transition metal (TM) atomic ten-rings consist of Cu atoms exclusively. In Fig. 2 sections of MI and MII are shown (for BI and BII see Ref. [16,23]). In contrast to BII and MII the models BI and MI display a central atom in the mixed atomic ten-rings. In the following we will see that this difference does not alter the PIXE profiles because the atomic density of the channeling planes is not changed significantly.

The PIXE data were measured at room temperature with a beam of  $3 \text{ MeV } ^4\text{He}^+$ -ions which had an angular spread of  $\pm 0.05^\circ$  due to the experimental beam geometry. The mosaic spread of the sample as determined by X-ray diffraction amounted to  $0.07^\circ$  (FWHM). From these measurements the presence of the microtwinned (5,7) approximant phase [30,31], which exhibits almost the same structure as the decagonal phase, can be excluded. Two angular scans were run: An axial one across the decagonal axis and a planar one inclined by  $5^\circ$  to the decagonal axis [21]. The experimental PIXE yield profiles are presented in Fig. 4.

To compare the four models with the experimental data Monte-Carlo channeling simulations have been performed. The principles of the simulations are described in [32]; a detailed outlay of channeling simulations for ordinary crystals is Ref. [33,34]. For simulations of PIXE profiles in quasicrystals see [20]. Since X-ray cross-sections are strongly dependent on the ion energy it is important to take the ion energy loss into account. For channeled ions we have used the approximation of van Vliet [35]. Stopping powers for non-channeled He ions are found in [36], ionization cross sections are tabulated in [37].

The simulation results of the minimum yield  $\chi_{\min}$  for the ion incidence in a channeling direction and the halfwidth

(HWHM)  $\Psi_{\frac{1}{2}}$  of the yield profile are documented in Tab. I for the axial case and in Tab. II for the planar case. The models BI, MI, BII and MII do not differ significantly in the axial PIXE profiles. In comparison to experiment (Tab. I) the values for  $\chi_{\min}$  are too low and almost identical for all three atomic species, whereas the experimental sequence is  $\chi_{\min,\text{Al}}$ ,  $\chi_{\min,\text{Co}}$  and  $\chi_{\min,\text{Cu}}$ .  $\Psi_{\frac{1}{2}}$  is in the experimental range for all models. So one has to summarize that in the axial case the four models are not distinguishable, the  $\Psi_{\frac{1}{2}}$  values are good but the  $\chi_{\min}$  values are much too low.

In the planar case the calculated PIXE-profiles are too deep, but in addition the  $\Psi_{\frac{1}{2}}$  values for all of the atomic species are too small. In contrast to the experimental data the Cu- and Co-profiles of BI and BII are not distinguishable. For MI and MII the simulations produce the correct experimental sequence of  $\chi_{\min,\text{Al}}$  as the lowest one, then  $\chi_{\min,\text{Co}}$  and finally  $\chi_{\min,\text{Cu}}$ .

The question remains whether the too deep PIXE-profiles and the too small  $\Psi_{\frac{1}{2}}$  in the planar case are explained by phason disorder, as up to now the simulations were performed on perfect model quasicrystals.

In [23] we introduced phason flips in one of the Burkoff models. With these flips we constructed four configurations of MII containing different amounts of phasons. As in the case of PIXE the profiles of MI and MII are very similar we expect that the results for a randomized MI model will not differ much from those of a randomized MII. To characterize the phason degree of disorder we use the deviation of the coordinates in perpendicular space with respect to the ideal quasicrystal. The phason degree of disorder, denoted  $u_{\text{ph}}$  in the following, is set to 1 for the maximally randomized configuration ( $\langle x^{\perp 2} \rangle_{\text{max}}$ ) and to 0 for the phason free one ( $\langle x^{\perp 2} \rangle_{\text{qc}}$ ), leading to the relation

$$u_{\text{ph}} = \frac{\langle x^{\perp 2} \rangle - \langle x^{\perp 2} \rangle_{\text{qc}}}{\langle x^{\perp 2} \rangle_{\text{max}} - \langle x^{\perp 2} \rangle_{\text{qc}}} . \quad (1)$$

In the simulations each model quasicrystal consists of six randomized quasiperiodic layers over which the phason disorder is averaged to obtain  $u_{\text{ph}}$ . In Fig. 3 both the results for the axial and for the planar case are presented. With  $u_{\text{ph}}$  also  $\chi_{\min}$  is increasing. The values of  $\Psi_{\frac{1}{2}}$  are decreasing with increasing  $u_{\text{ph}}$  in the axial case. In the planar case they remain approximately constant. Obviously phason disorder has similar effects on PIXE-profiles as phonon disorder.

All the simulations mentioned above have been performed with an angular spread of  $\pm 0.05^\circ$  which is fixed by the beam geometry of the experiment; in reality the angular spread is slightly higher, due to e.g. the mosaic spread of the quasicrystal. A higher angular spread increases  $\chi_{\min}$ , broadens the profile and improves agreement with the experimental data. This is demonstrated in Fig. 4 where the calculated PIXE-profile for a MII crystal with  $u_{\text{ph}} = 0.27$  and an angular spread of  $\pm 0.1^\circ$  are

compared directly with the measurements. Since  $\chi_{\min}$  for Cu and Co is somewhat deeper in the simulation (Tab. I) than in the experiment for the axial case it has been adjusted by a marginal offset [38] to show that  $\Psi_{\frac{1}{2}}$  is in agreement with the experiment (Fig. 4). The offset is justified by the fact that the PIXE yields of Cu and Co result from depths up to 4  $\mu\text{m}$ ; from these depths the X-ray contribution from dechanneled ions is considerable and may vary strongly, if the sources for dechanneling, e.g. the size of thermal displacements are not known exactly. Axial channeling is more sensitive to this effect than planar channeling.

With these results and the RBS calculations [27] we come to the conclusion that the AlCuCo quasicrystal used in the experiment is a random tiling. Other profile changing effects like vacancies or microcrystalline states lead to different results in the RBS-profiles, which we will discuss in a forthcoming paper [27]. In the case of planar channeling also chemical disorder between the transition metal atoms can lead to the contradictory result that  $\chi_{\min, \text{Cu}}$  is deeper than  $\chi_{\min, \text{Co}}$ .

We thank G. Groos and A. Rüdinger for helpful discussion. This work has been supported by the Deutsche Forschungsgemeinschaft under project numbers CA 122/3-2 and RO 924/4-1.

- 
- [1] N.G. De Bruijn, Math. Proc. **A84**, 39 (1981).  
[2] R. Klitzing, M. Schlottmann, and M. Baake, Int. J. Mod. Phys. B **7**, 1455 (1993).  
[3] P.A. Kalugin and A. Katz, Europhys. Lett. **21**, 921 (1993).  
[4] A. Trub and H.-R. Trebin, J. Phys. I France **4**, 1855 (1994).  
[5] A. Rüdinger and H.-R. Trebin, J. Phys. A **27**, 7981 (1994).  
[6] R. Blüher, P. Scharwächter, W. Frank and H. Kronmüller Phys. Rev. Lett. **80**, 1014 (1998).  
[7] O. Entin-Wohlman, M. Kleman, and A. Pavlovitch, J. Phys. France **49**, 587 (1988).  
[8] C. Henley, in Quasicrystals - The State of the Art, edited by D.P. DiVincenzo and P.J. Steinhard, Directions in Condensed Matter Physics Vol. 11 (World Scientific, Singapore, 1991)  
[9] A.R. Kortan, R.S. Becker, F.A. Thiel, and H.S. Chen, Phys. Rev. Lett. **64**, 200 (1990).  
[10] K. Hiraga, W. Sun, and F.J. Lincoln, Jpn. J. Mod. Phys. **30**, L301 (1991).  
[11] W. Steurer and K.H. Kuo, Philos. Mag. Lett. **62**, 175 (1990).  
[12] W. Steurer, Acta. Crystallogr. Sect. B **46**, 703 (1990).  
[13] A.R. Kortan, F.A. Thiel, H.S. Chen, A.P. Tsai, A. Inoue, and T. Masumoto, Phys. Rev. B **40**, 9397 (1989).  
[14] For some samples a doubling of the stacking period is reported [11,13], which we do not take into account here.  
[15] S.E. Burkov, Phys. Rev. Lett. **67**, 614 (1991).  
[16] S.E. Burkov, Phys. Rev. B **47**, 12325 (1993).  
[17] H.D. Carstanjen, R.-M. Emrick, R. Grunwald, D. Plachke and R. Wittmann Phys. Rev. B **45**, 10822 (1992)  
[18] For an overview on channeling in quasicrystals see: D. Plachke and H.D. Carstanjen in Quasicrystals – An Introduction to the Structure, Physical Properties and Applications of Quasicrystalline Alloys, edited by J.B. Suck, M. Schreiber and P. Häussler (Springer, Heidelberg (1998 to be published))  
[19] H.D. Carstanjen, R.-M. Emrick, T. Kupke, D. Plachke and R. Wittmann Nucl. Inst. Meth. B **67**, 173 (1992)  
[20] D. Plachke, PhD thesis, University of Stuttgart (1998)  
[21] D. Plachke, T. Kupke, H.D. Carstanjen und R.-M. Emrick, J. Non-Cryst. Solids **153&154**, 72-76 (1993)  
[22] F. Frey and W. Steurer, J. Non-Cryst. Solids **153-154**, 600 (1993).  
[23] G. Zeger and H.-R. Trebin, Phys. Rev. B **54**, R720 (1996).  
[24] One variant of the Burkov model introduced by Krajčí *et al.* for the interpretation of photoemission data shows a reversed Cu/Co ordering in contrast to MII [25]. The reason may be that the influence of phason disorder on the data has not been examined. In a recent paper Cockayne and Widom proposed a ternary model for Al-Cu-Co with a Cu/Co ordering similar to MII [26].  
[25] M. Krajčí, J. Hafner and M. Mihalkovič, Phys. Rev. B **56**, 3072 (1997)  
[26] E. Cockayne and M. Widom, Phys. Rev. Lett. **81**, 598 (1998)  
[27] G. Zeger and H.-R. Trebin, in preparation  
[28] The position of each atom is expressed as an integer linear combination of the vectors of a regular pentagonal star. These atomic coordinate quintuples  $\mathbf{n} \in \mathbb{Z}^5$  can be arranged into five translation classes  $T = \sum_{i=1}^5 n_i \bmod 5$ .  
[29] A. Katz and M. Duneau, J. Physique **47**, 181 (1986).  
[30] R. Wittmann, M. Fettweis, P. Launois, R. Reich and F. Dnoyer, Phil. Mag. Lett. **71**, 147 (1995)  
[31] M. Kalning, S. Kek, B. Burandt, W. Press and W. Steurer, J. Phys. Cond. Matt. **6**, 6177 (1994)  
[32] T. Kupke, U. Peschke, H.D. Carstanjen and H.-R. Trebin Phys. Rev. B **43**, 13758 (1991)  
[33] J.H. Barrett Phys. Rev. B **3**, 1527 (1971)  
[34] H.D. Carstanjen and R. Sizmann Radiat. Eff. **12**, 211 (1972)  
[35] D. van Vliet Phys.Stat.Sol.A2, 521(1970)  
[36] ZIEGLER, J. F.: *The stopping and range of He and H*, 4 *Handbook of Stopping Power*. Pergamon Press, 1985.  
[37] MAYER, J. W. E. RIMINI : *Ion Beam Handbook for Material Analysis*. Academic Press, New York, 1977.  
[38] The offset is the difference between simulated  $\chi_{\min, \text{sim}}$  and experimental  $\chi_{\min, \text{exp}}$  with  $\chi_{\text{of}} = \chi_{\min, \text{exp}} - \chi_{\min, \text{sim}}$ .

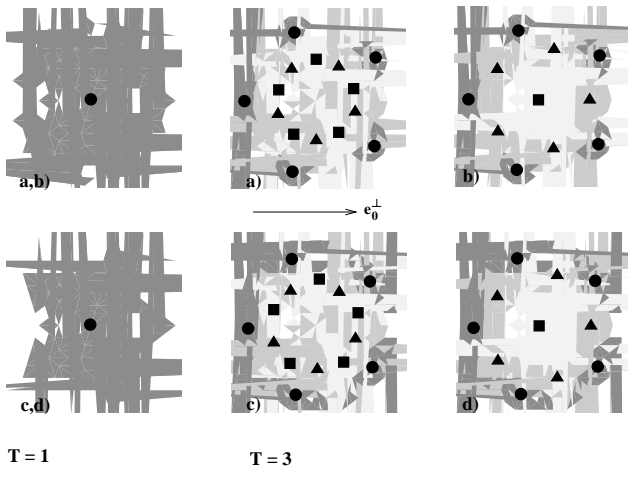


FIG. 1. The atomic surfaces of the first layer and translational class  $T=1,3$  for the three models: (a) BI, (b) MI, (c) BII and (d) MII. Note that the surfaces of  $T=1$  are identical for BI/MI and BII/MII, respectively. The surfaces of  $T=2,4$  belong to layer 2 and are a rotated copy.

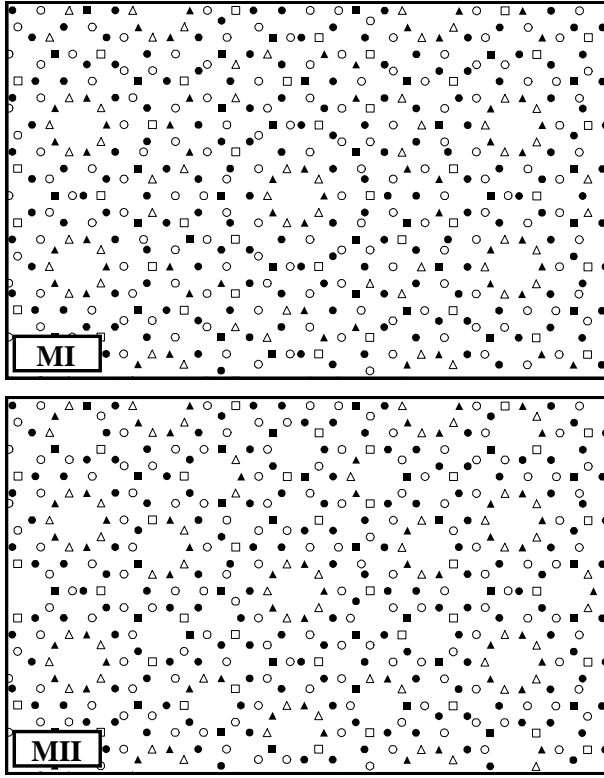


FIG. 2. Above: Part of the AlCuCo model MI; below: Part of model MII. The atomic positions in the two layers are projected along the decagonal axis, layer one with filled and layer two with empty symbols. The symbols are:  $\square$  for Co,  $\Delta$  for Cu and  $\circ$  for Al.

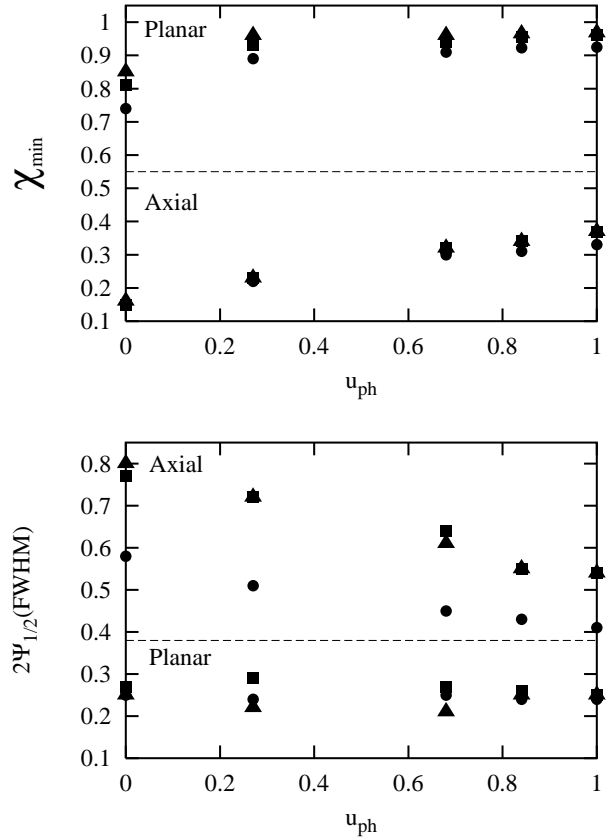


FIG. 3. Simulated  $\chi_{\min}$  (above) and  $\Psi_{1/2}$  (below) for different phason disorder for MII both in the planar and the axial case with an angular spread of  $\pm 0.05^\circ$ .

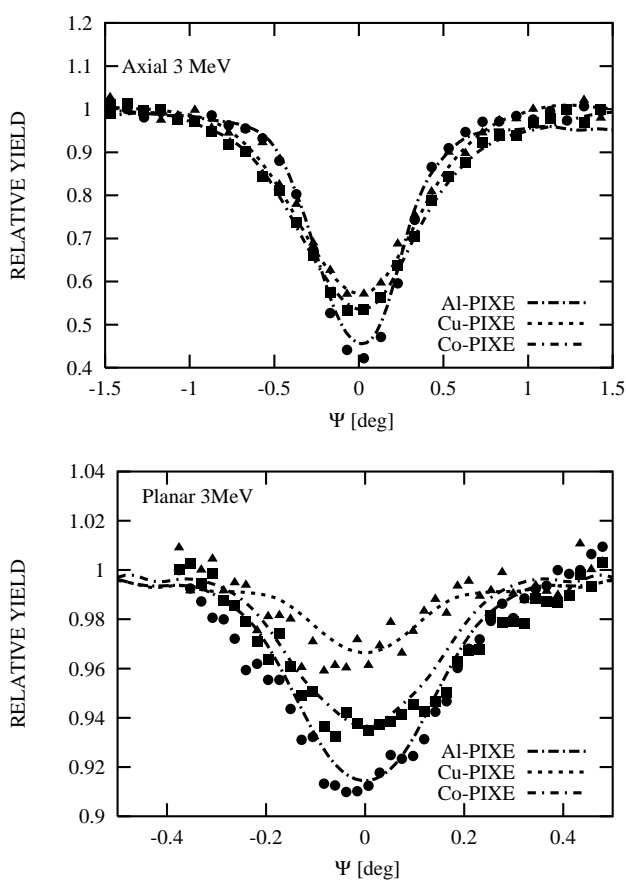


FIG. 4. X-ray yield profiles as obtained from angular scans across the decagonal axis (above) and the main planar system (below). The experimental data are shown for T-phase  $\text{Al}_{62}\text{Cu}_{20}\text{Co}_{15}\text{Si}_3$  with the same symbols as in Fig. 2 for the elements. The lines represent the calculated profiles for the MII model with a phason disorder of 0.27 and an angular spread of  $\pm 0.1^\circ$ . The profiles for Co and Cu in the axial case (above) have been adjusted by an offset of 0.15 and 0.19 respectively [38].

	Al-yield		Cu-yield		Co-yield	
	$\chi_{\min}$	$2\Psi_{\frac{1}{2}}$ [deg]	$\chi_{\min}$	$2\Psi_{\frac{1}{2}}$ [deg]	$\chi_{\min}$	$2\Psi_{\frac{1}{2}}$ [deg]
BI	0.15	0.56	0.14	0.76	0.15	0.71
MI	0.12	0.55	0.13	0.76	0.14	0.72
BII	0.15	0.55	0.15	0.75	0.15	0.70
MII	0.15	0.58	0.16	0.80	0.15	0.77
MII*	0.45	0.59	0.38	0.82	0.38	0.83
Experiment	0.42	0.58	0.57	0.78	0.53	0.81

TABLE I. Axial Channeling: Simulated  $\chi_{\min}$  and  $2\Psi_{\frac{1}{2}}$  (FWHM) for the four models without phason disorder compared with the experimental data with an angular spread of  $\pm 0.05^\circ$ . MII\*: Data for MII with  $u_{\text{ph}} = 0.27$  and an angular spread of  $\pm 0.1^\circ$  (see also Fig.4).

	Al-yield		Cu-yield		Co-yield	
	$\chi_{\min}$	$2\Psi_{\frac{1}{2}}$ [deg]	$\chi_{\min}$	$2\Psi_{\frac{1}{2}}$ [deg]	$\chi_{\min}$	$2\Psi_{\frac{1}{2}}$ [deg]
BI	0.74	0.23	0.83	0.23	0.83	0.23
MI	0.74	0.26	0.84	0.26	0.82	0.26
BII	0.75	0.23	0.84	0.23	0.84	0.23
MII	0.74	0.25	0.85	0.25	0.81	0.27
MII*	0.91	0.32	0.96	0.29	0.94	0.36
Experiment	0.91	0.37	0.96	0.32	0.94	0.41

TABLE II. Planar Channeling Simulated  $\chi_{\min}$  and  $2\Psi_{\frac{1}{2}}$  (FWHM) for the four models compared with the experimental data with an angular spread of  $\pm 0.05^\circ$ . MII\*: Data for MII with  $u_{\text{ph}} = 0.27$  and an angular spread of  $\pm 0.1^\circ$  (see also Fig.4).